Supporting Information

Highly efficient near ultraviolet organic light-emitting diode based on a meta-linked donor-acceptor molecule

Haichao Liu,[ab] Qing Bai,[ab] Liang Yao,[ab] Haiyan Zhang,[b] Hai Xu,[b] Shitong Zhang,[ab] Weijun Li,[a] Yu Gao,[ab] Jinyu Li,[ab] Ping Lu,[ab] Hongyan Wang,[b] Bing Yang,*[ab] and Yuguang Ma[c]

[a] State Key Laboratory of Supramolecular Structure and Materials, Jilin University, Changchun, 130012, P. R. China

[b] College of Chemistry, Jilin University, Changchun, 130012, P. R. China

[c] State Key Laboratory of Luminescent Materials and Devices, Institute of Polymer Optoelectronic Materials and Devices, South China University of Technology, Guangzhou, 510640, P. R. China

*Corresponding Author. E-mail: yangbing@jlu.edu.cn

Contents

S-I Characterization and Measurements

General information**:** The ^{1}H NMR spectra were recorded on AVANCE 500 spectrometers at 298 K by utilizing deuterated dimethyl sulfoxide (DMSO) as solvents and tetramethylsilane (TMS) as a standard. The compounds were characterized by a Flash EA 1112, CHNS-O elemental analysis instrument. The MALDI-TOF-MS mass spectra were recorded using an AXIMA-CFR^{TM} plus instrument.

Photophysical measurements**:** UV-vis absorption spectra were recorded on a UV-3100 spectrophotometer. Fluorescence measurements were carried out with a RF-5301PC. PL efficiencies in solvents were measured with a UV-3100 and a RF-5301PC, relative to quinine sulfate. PL efficiencies in films were measured on the quartz plate using an integrating sphere apparatus.

Lippert-Mataga model**:** The influence of solvent environment on the optical property of our compounds can be understood using the Lippert-Mataga equation, a model that describes the interactions between the solvent and the dipole moment of solute:

$$hc(\nu_{\mathrm{a}} - \nu_{\mathrm{f}}) = hc(\nu_{\mathrm{a}}^0 - \nu_{\mathrm{f}}^0) - \frac{2(\mu_e - \mu_g)^2}{\mathrm{a}^3} f(\varepsilon, n)$$

where f is the orientational polarizability of solvents, μ_{e} is the dipole moment of excited state, μ_{g} is the dipole moment of ground state; a is the solvent cavity (Onsager) radius, ε and n are the solvent dielectric and the solvent refractive index, respectively.

Quantum chemical calculations**:** All the density functional theory (DFT) calculations were carried out using Gaussian 09 (version D.01) package on a PowerLeader cluster.[1] The ground-state geometry was fully optimized using DFT with B3LYP hybrid functional at the basis set level of 6-31G(d, p). The excited-state geometry was optimized by time-dependent density functional theory (TD-DFT) with the B3LYP functional at the same basis set level. The absorption and emission properties were obtained using TD-M06-2X)/6-31G(d, p) at the ground state and excited state geometries, respectively.

Electrochemical characterization**:** Cyclic voltammetry (CV) was performed with a BAS 100W Bioanalytical Systems, using a glass carbon disk (Φ = 3 mm) as the working electrode, a platinum wire as the auxiliary electrode with a porous ceramic wick, Ag/Ag$^+$ as the reference electrode, standardized for the redox couple ferricinium/ferrocene. All solutions were purged with a nitrogen stream for 10 min before measurement. The procedure was performed at room temperature and a nitrogen atmosphere was maintained over the solution during measurements.

Thermal stability measurements**:** Thermal gravimetric analysis (TGA) was undertaken on a PerkinElmer thermal analysis system at a heating rate of 10 °C min^{-1}

and a nitrogen flow rate of 80 mL min^{-1}. Differential scanning calorimetry (DSC) analysis was carried out using a NETZSCH (DSC-204) instrument at 10 °C min^{-1} while flushing with nitrogen.

***Device fabrication and performances*:** The EL devices were fabricated by vacuum deposition of the materials at indium tin oxide (ITO) glass. All of the organic layers were deposited at a rate of 1.0 Å s^{-1}. The cathode was deposited with LiF (1 nm) at a deposition rate of 0.1 Å s^{-1} and then capping with Al metal (100 nm) through thermal evaporation at a rate of 4.0 Å s^{-1}.

EQE was calculated according to the formula below:[2]

$$\mathrm{EQE} = \frac{\pi \cdot \mathrm{L} \cdot \mathrm{e}}{683 \cdot \mathrm{I} \cdot \mathrm{h} \cdot \mathrm{c}} \cdot \frac{\int_{380}^{780} \mathrm{I}(\lambda) \cdot \lambda \mathrm{d}\lambda}{\int_{380}^{780} \mathrm{I}(\lambda) \cdot \mathrm{K}(\lambda) \mathrm{d}\lambda}$$

where L (cd m^{-2}) is the total luminance of device, I (A) is the current flowing into the EL device, λ (nm) is EL wavelength, I(λ) is the relative EL intensity at each wavelength and obtained by measuring the EL spectrum, K(λ) is the Commision International de L'Eclairage chromaticity (CIE) standard photopic efficiency function, e is the charge of an electron, h is the Planck's constant, c is the velocity of light.

The electroluminescence (EL) spectra and Commission International de L'Eclairage (CIE) coordination of these devices were measured by a PR650 spectra scan spectrometer. The luminance-current density-voltage characteristics were recorded simultaneously with the measurement of the EL spectra by combining the spectrometer with a Keithley model 2400 programmable voltage-current source. All measurements were carried out at room temperature under ambient conditions.

S-II Synthesis

All the reagents and solvents used for the synthesis were purchased from Aldrich or Acros and used as received. All reactions were performed under nitrogen atmosphere.

***2-(3-Bromo-phenyl)-1-phenyl-1H-phenanthro[9,10-d]imidazole* (mBr -PPI)**.

A mixture of phenanthrenequinone (10.0 mmol), 3-bromo-benzaldehyde (10.0 mmol), aniline (40.0 mmol), ammonium acetate (50.0 mmol), and acetic acid (30 mL) was refluxed under nitrogen at 120 ˚C oil bath for 2 h. After the mixture was cooled down and filtered, the solid product was washed with a 50 mL acetic acid/water mixture (1:1) and 50 mL water, dissolved in CH_2Cl_2 and dried in $MgSO_4$ overnight. It was then purified by chromatography using the mixture of CH_2Cl_2/petroleum ether as an eluent and pure dry white product is obtained (3.59 g, yield 80%). MS (ESI): MW 449.3, m/z 449.7 (M^+). ^1H NMR (500 MHz, DMSO): δ 8.93 (d, J = 8.3 Hz, 1H), 8.88 (d, J = 8.3 Hz, 1H), 8.70 (dd, J = 7.9, 1.0 Hz, 1H), 7.82 – 7.65 (m, 8H), 7.62 – 7.51 (m, 3H), 7.40 – 7.26 (m, 2H), 7.10 (d, J = 7.7 Hz, 1H).

***Diphenyl-[3'-(1-phenyl-1H-phenanthro[9,10-d]imidazol-2-yl)-biphenyl-4-yl]-amine* (mTPA-PPI).**

A mixture of mBr-PPI (4.20 mmol), N,N-diphenyl-4-(4,4,5,5-tetramethyl-1,3,2-dioxaborolan-2-yl)aniline (4.25 mmol), sodium carbonate (36 mmol), toluene (27 mL), absolute alcohole (13.5 ml) and deionized water (18 mL), with $Pd(PPh_3)_4$ (98 mg) acting as catalyst was refluxed at 90 ˚C for 48 h under nitrogen. After the mixture was cooled down, 40 mL water was added to the resulting solution and the mixture was extracted with CH_2Cl_2 for several times. The organic phase was dried over Na_2SO_4. After filtration and solvent evaporation, the liquid was purified by chromatography using the mixture of CH_2Cl_2/petroleum ether as the eluent to afford a white solid (1.68 g, yield 65%). MS (ESI): MW 613.8, m/z 614.5(M^+). ^1H NMR (500 MHz, DMSO): δ 8.95 (d, J = 8.4 Hz, 1H), 8.90 (d, J = 8.4 Hz, 1H), 8.72 (d, J = 7.8 Hz, 1H), 7.79 (dd, J = 9.4, 5.0 Hz, 3H), 7.76 – 7.68 (m, 5H), 7.67 – 7.62 (m, 2H), 7.57 (t, J = 7.6 Hz, 1H), 7.46 (t, J = 7.8 Hz, 1H), 7.39 – 7.32 (m, 7H), 7.14 (d, J = 8.2 Hz, 1H), 7.09 (dd, J = 17.5, 7.8 Hz, 6H), 7.02 (d, J = 8.6 Hz, 2H). ^{13}C NMR (500 MHz, CDCl3): δ 150.837, 147.685, 147.398, 140.440, 138.937, 137.407, 134.434, 130.820, 130.245, 129.795, 129.333, 129.259, 128.758, 128.325, 128.165, 127.956, 127.784, 127.759, 127.336, 127.230, 127.014, 126.300, 125.675, 124.941, 124.496, 124.155, 123.804, 123.138, 123.062, 123.020, 122.868, 120.914. Elemental analysis. Found: C, 88.10; H, 5.18; N,6.83. Calc. for $C_{45}H_{31}N_3$: C, 88.06; H, 5.09; N, 6.85%.

S-III Tables and figures

Table S1 The ground state and excited state geometries in PPI, TPA-PPI and mTPA-PPI

Molecules	Ground state	Excited state
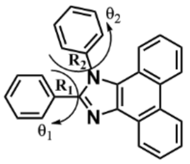 PPI	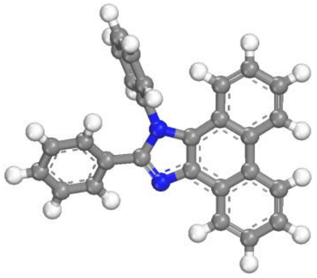	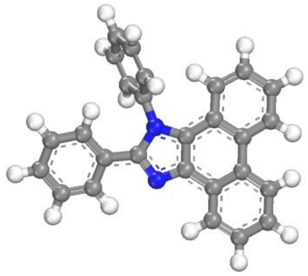
Optimized geometry parameters	R_1=1.4742Å; R_2=1.4333Å; θ_1=-30.34˚; θ_2=-75.19˚	R_1=1.4453Å; R_2=1.4323Å; θ_1=-11.50˚; θ_2=-59.14˚
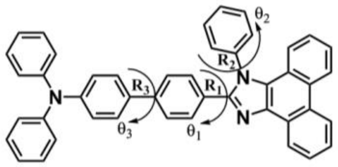 TPA-PPI	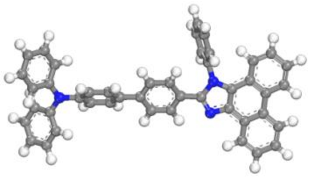	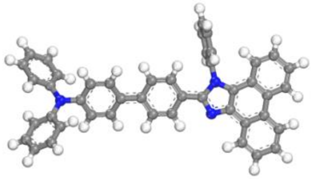
Optimized geometry parameters	R_1=1.4720Å; R_2=1.4331Å; R_3=1.4806Å; θ_1=-30.74˚; θ_2=-78.39˚; θ_3=-35.50˚	R_1=1.4366Å; R_2=1.4294Å; R_3=1.4462Å; θ_1=-7.22˚; θ_2=-85.82˚; θ_3=-14.79˚
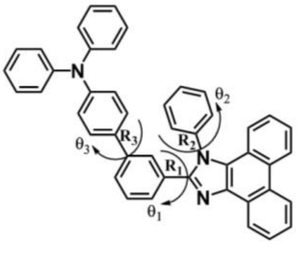 mPA-PPI	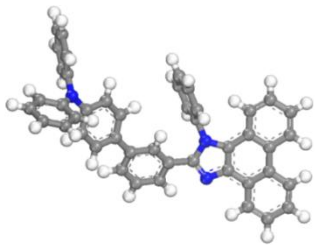	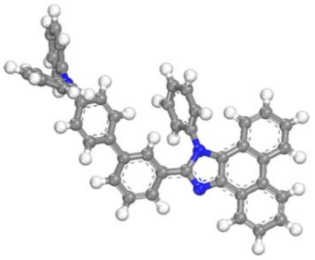
Optimized geometry parameters	R_1=1.4746Å; R_2=1.4331Å; R_3=1.4843Å; θ_1=-32.04˚; θ_2=-74.49˚; θ_3=37.35˚	R_1=1.4358Å; R_2=1.4129Å; R_3=1.4784Å; θ_1=-13.75˚; θ_2=-53.74˚; θ_3=30.95˚

Table S2 Absorption and emission properties of PPI, TPA-PPI and mTPA-PPI in vacuum gas phase by TDDFT-M06-2X/6-31G (d, p) at the optimized geometries by B3LYP/6-31G (d, p)

Molecules	Abs/Emi	Electronic transition	λ_{cal} (nm)	Excited-state character	λ_{exp} (nm) in Hexane
PPI	Abs	$S_0 \rightarrow S_1$	299	$\pi_A \rightarrow \pi_A^*$	316
(A)	Emi	$S_1 \rightarrow S_0$	338	$\pi_A \rightarrow \pi_A^*$	364
TPA-PPI	Abs	$S_0 \rightarrow S_1$	323	$\pi_{D-A} \rightarrow \pi_{D-A}^*$	365
(D-A)	Emi	$S_1 \rightarrow S_0$	378	$\pi_{D-A} \rightarrow \pi_{D-A}^*$	406
mTPA-PPI	Abs	$S_0 \rightarrow S_1$	303	$\pi_A \rightarrow \pi_A^*$ $\pi_D \rightarrow \pi_D^*$	330
(D-A)	Emi	$S_1 \rightarrow S_0$	334	$\pi_A \rightarrow \pi_A^*$	367

Table S3 Detailed absorption and emission peak positions of PPI in different solvents

solvents	$f(\varepsilon,n)$	PPI λ_a (nm)	PPI λ_f (nm)	PPI v_a-v_f (cm^{-1})	η_{PL}[a] (%)
Hexane	0.0012	316	364	4173	37
Triethylamine	0.048	314	365	4450	25
Butyl ether	0.096	313	366	4626	44
Isopropyl ether	0.145	312	365	4654	37
Ethyl ether	0.167	310	366	4936	40
Ethyl acetate	0.200	312	368	4877	46
Tetrahydrofuran	0.210	311	369	5054	54
Dimethyl formamide	0.276	310	373	5448	65
Acetone	0.284	---	373	---	20
Acetonitrile	0.305	307	372	5692	45

[a] η_{PL} values in different solvents were measured using a 0.1 mol/L H_2SO_4 solution of quinine sulfate as reference (0.546).

Table S4 Detailed absorption and emission peak positions of mTPA-PPI in different solvents

solvents	$f(\varepsilon,n)$	mTPA-PPI λ_a (nm)	mTPA-PPI λ_f (nm)	mTPA-PPI v_a-v_f (cm^{-1})	η_{PL} [a] (%)
Hexane	0.0012	330	367	3055	41
Triethylamine	0.048	330	369	3203	26
Butyl ether	0.096	329	369	3295	48
Isopropyl ether	0.145	329	385	4421	42
Ethyl ether	0.167	328	386	4581	48
Ethyl acetate	0.200	327	406	5950	51
Tetrahydrofuran	0.210	329	407	5825	55
Dimethyl formamide	0.276	328	436	7552	62
Acetone	0.284	327	425	7052	21
Acetonitrile	0.305	323	437	8077	46

[a] η_{PL} values in different solvents were measured using a 0.1 mol/L H_2SO_4 solution of quinine sulfate as reference (0.546).

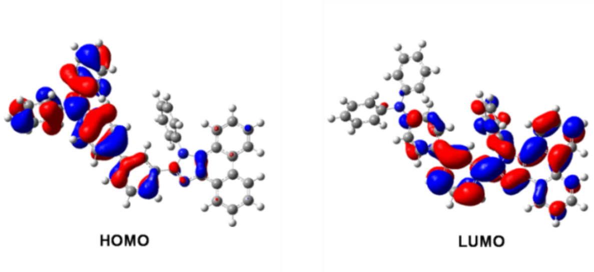

Figure S1 HOMO and LUMO of mTPA-PPI at ground state.

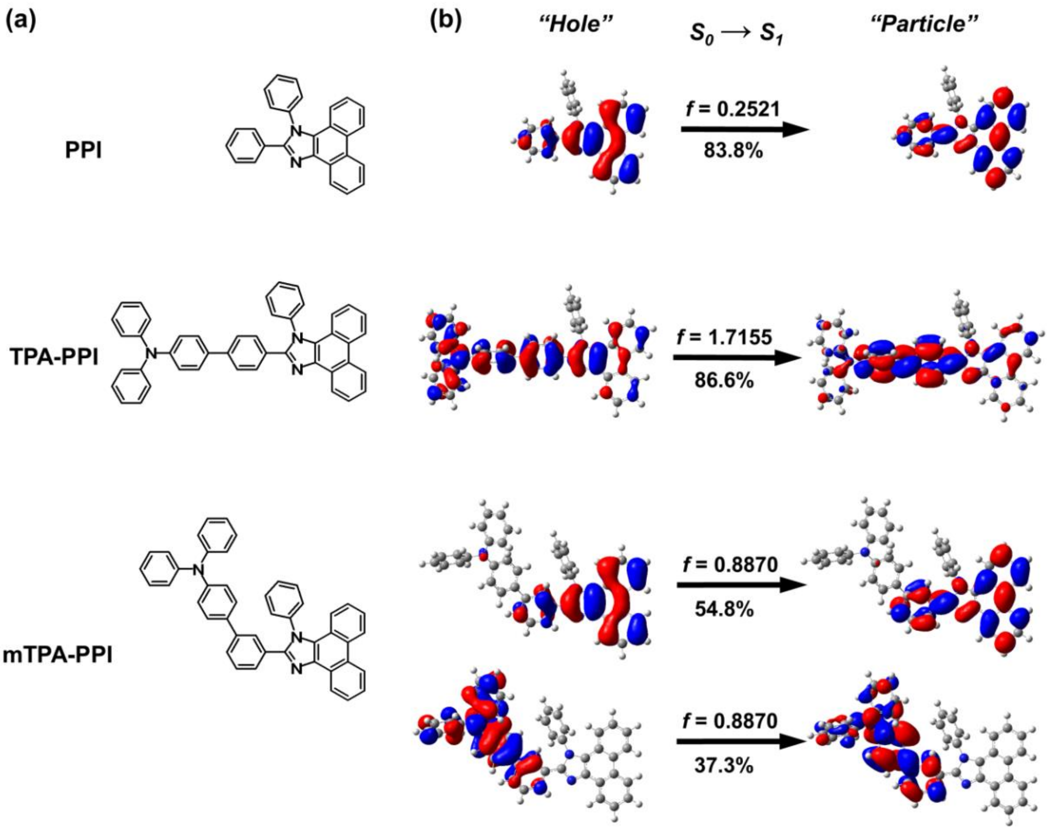

Figure S2 (a) Molecular structures. (b) NTO for $S_0 \rightarrow S_1$ absorption transition in PPI, TPA-PPI and mTPA-PPI. Herein, *f* represents for the oscillator strength, and the percentage weights of hole-particle are given for the $S_0 \rightarrow S_1$ absorption.

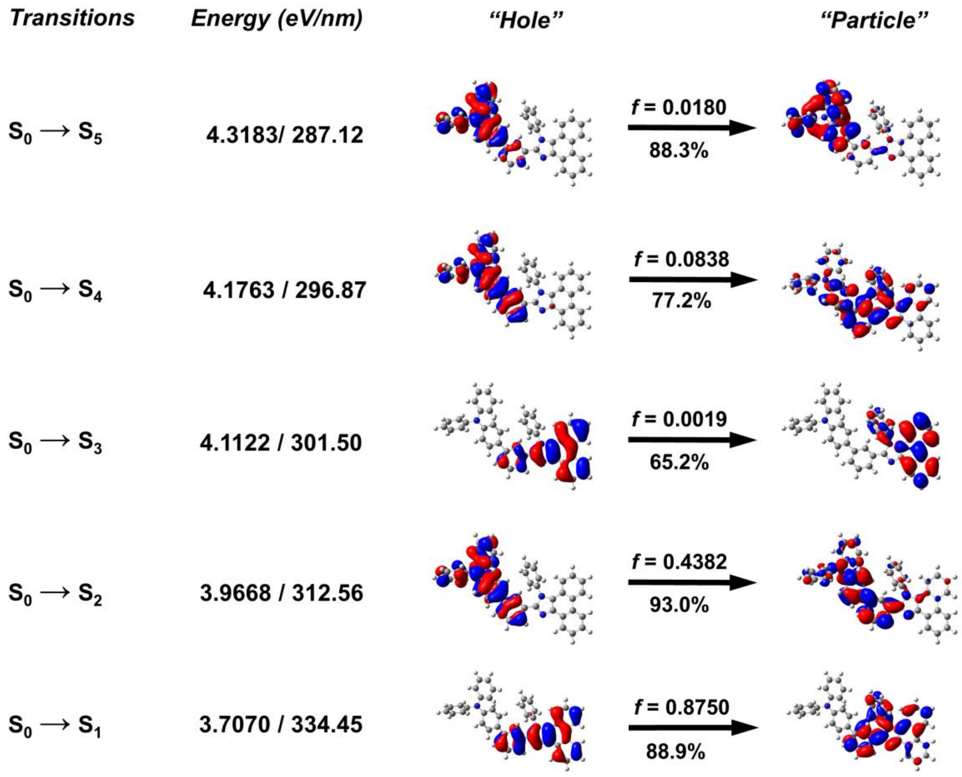

Figure S3 NTO for $S_0 \rightarrow S_n$ electronic transition character in mTPA-PPI. Herein, *f* represents for the oscillator strength, and the percentage weights of hole-particle are given for the $S_0 \rightarrow S_n$ transitions based on S_1 state geometry.

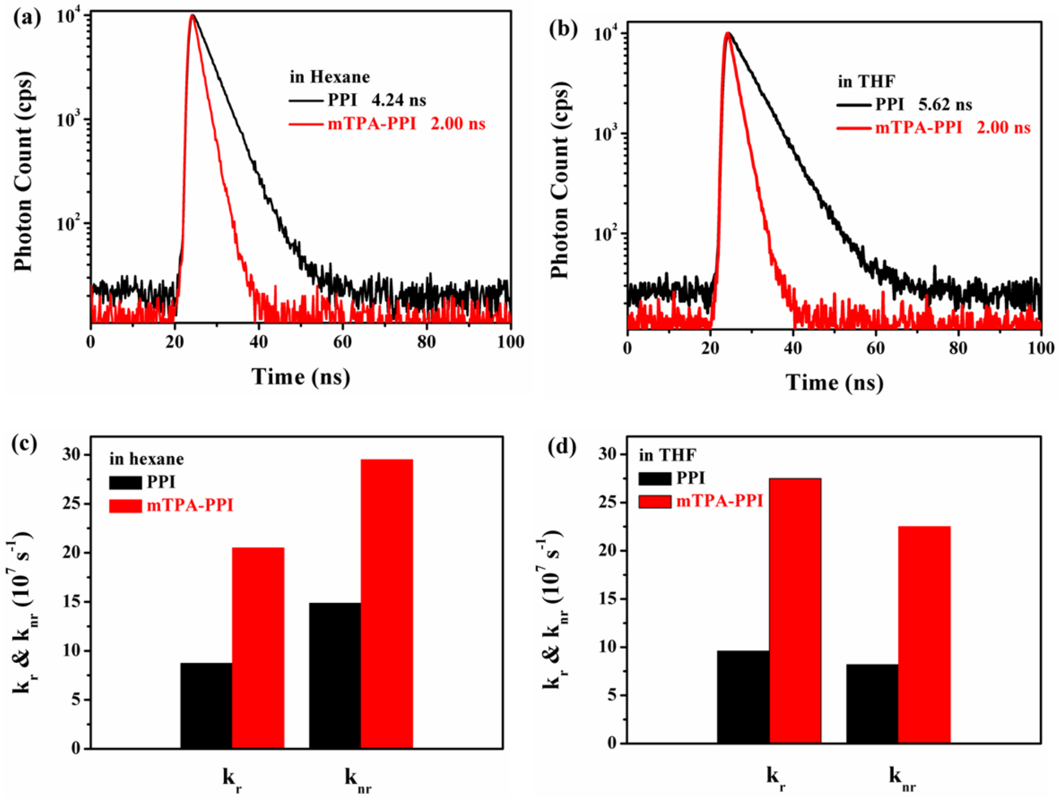

Figure S4 Lifetime measurement of PPI and mTPA-PPI (a) in hexane solution (b) in THF solution by using time-correlated single photon counting method under the excitation of a laser (280.2 nm) with 885.42 ps pulse width; The radiative transition rates (k_r) and non-radiative transition rates (k_{nr}) of PPI and mTPA-PPI (c) in hexane solution (d) in THF solution. Both PPI and mTPA-PPI show mono-exponential lifetime curve in hexane and THF, indicating a single emissive state species. Compared with PPI, the lifetime of mTPA-PPI is obviously shortened due to its enhanced k_r and k_{nr} in both hexane and THF.

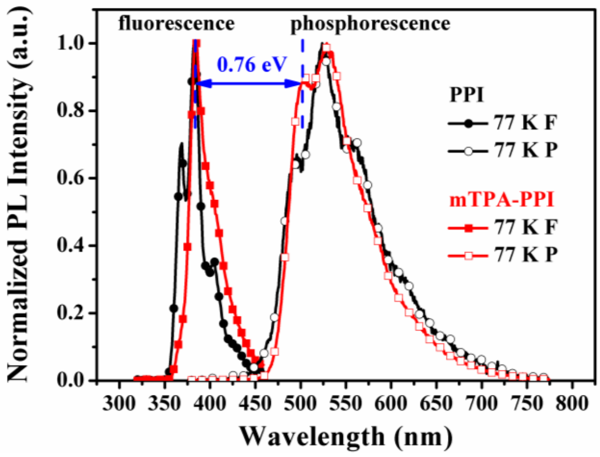

Figure S5 Low-temperature fluorescence (using RF-5301PC) and phosphorescence (using a LP 920) spectra at 77K of PPI and mTPA-PPI were measured in frozen THF matrix.

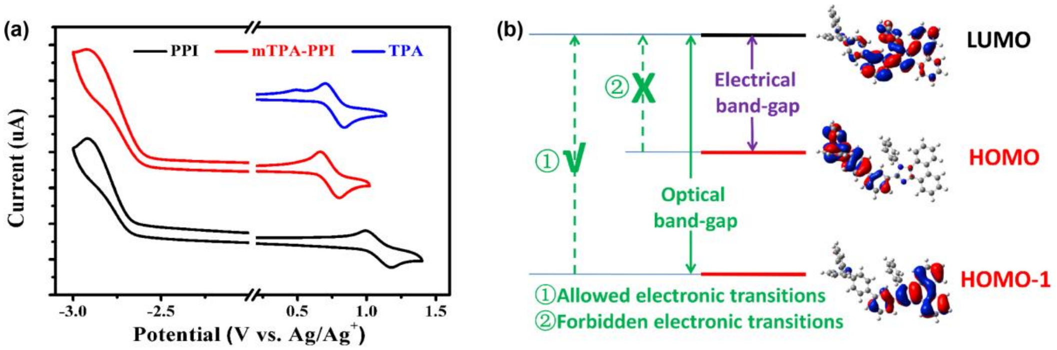

Figure S6 (a) The CV curves of PPI and mTPA-PPI. (b) Schematic diagram of design principle of mTPA-PPI.

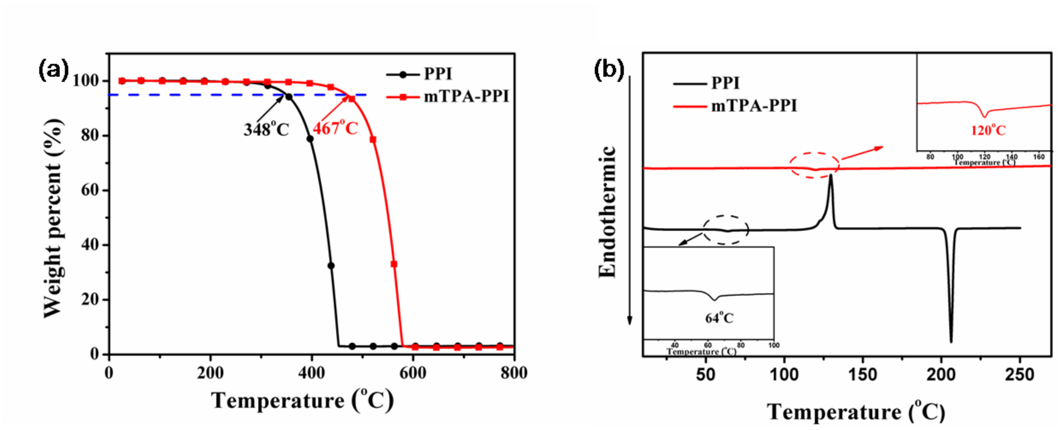

Figure S7 (a) TGA graph (b) DSC graph of PPI and mTPA-PPI.

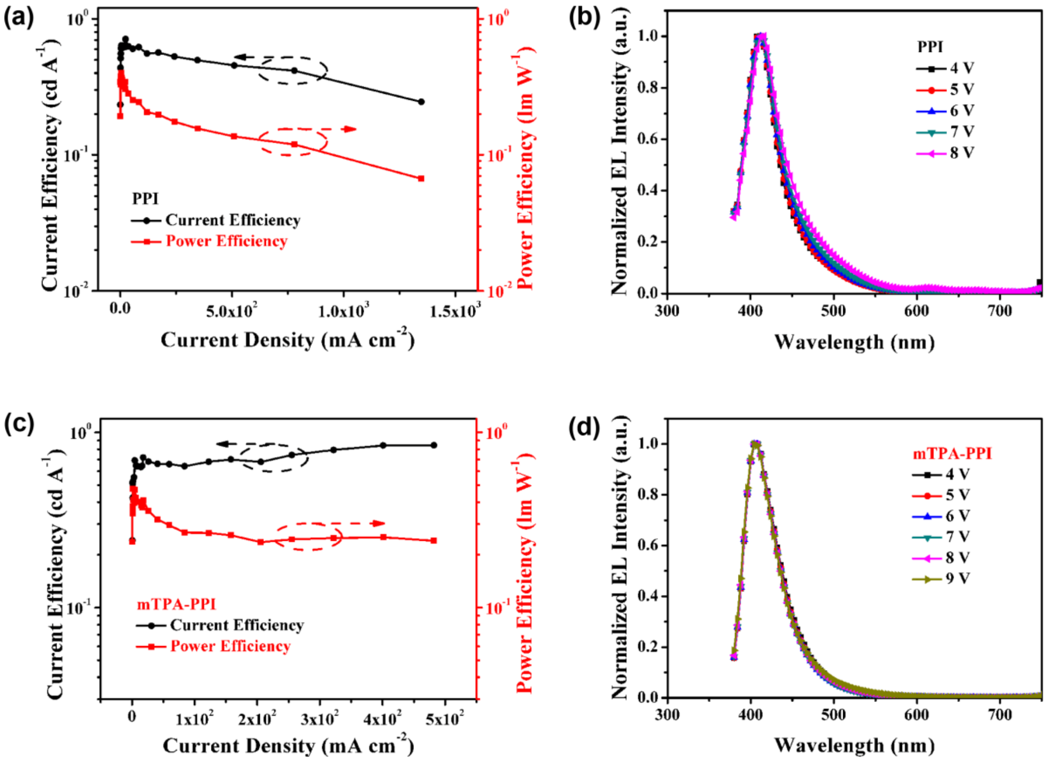

Figure S8 (a) The current efficiency-current density-power efficiency curve of multilayered OLED based on PPI. (b) The EL spectra of PPI based OLED at different driving voltages. (c) The current efficiency- current density -power efficiency curve of multilayered OLED based on mTPA-PPI. (d) The EL spectra of mTPA-PPI based OLED at different driving voltages.

Table S5 Key data summary of the mTPA-PPI-based device and other high-performance violet/NUV light-emitting devices

Emitters	$V_{\text{turn-on}}$ (V)	$LE_{\max}$ (cd A^{-1})	$PE_{\max}$ (lm W^{-1})	$EQE_{\max}$ (%)	$\lambda_{\text{EL, max}}$ (nm)	CIE (x,y)	ref
mTPA-PPI	3.2	0.84	0.48	3.33	404	(0.161, 0.049)	this work[a]
B2	2.5	—	—	3.6	374,392	—	[3] [a]
T2	2.5	—	—	2.8	402	—	[3] [a]
TB2	2.5	—	—	2.7	374,396	—	[3] [a]
Purine2	3.2	—	—	1.6	393	—	[4] [b]
SSM	—	1.8	—	2.56	408	(0.168,0.088)	[5] [a]
CzSiSF	4.8	0.32	—	0.48	410	—	[6] [a]
CzPySiSF	5.8	0.35	—	0.59	408	—	[6] [a]

[a] Non-doped devices. [b] Doped devices.

References

[1] M. J. Frisch, G. W. Trucks, H. B. Schlegel, G. E. Scuseria, M. A. Robb, J. R. Cheeseman, G. Scalmani, V. Barone, B. Mennucci, G. A. Petersson, H. Nakatsuji, M. Caricato, X. Li, H. P. Hratchian, A. F. Izmaylov, J. Bloino, G. Zheng, J. L. Sonnenberg, M. Hada, M. Ehara, K. Toyota, R. Fukuda, J. Hasegawa, M. Ishida, T. Nakajima, Y. Honda, O. Kitao, H. Nakai, T. Vreven, J.

A. Montgomery, Jr., J. E. Peralta, F. Ogliaro, M. Bearpark, J. J. Heyd, E. Brothers, K. N. Kudin, V. N. Staroverov, R. Kobayashi, J. Normand, K. Raghavachari, A. Rendell, J. C. Burant, S. S. Iyengar, J. Tomasi, M. Cossi, N. Rega, J. M. Millam, M. Klene, J. E. Knox, J. B. Cross, V. Bakken, C. Adamo, J. Jaramillo, R. Gomperts, R. E. Stratmann, O. Yazyev, A. J. Austin, R. Cammi, C. Pomelli, J. W. Ochterski, R. L. Martin, K. Morokuma, V. G. Zakrzewski, G. A. Voth, P. Salvador, J. J. Dannenberg, S. Dapprich, A. D. Daniels, Ö. Farkas, J. B. Foresman, J. V. Ortiz, J. Cioslowski and D. J. Fox, *Gaussian 09, Revision D.01*, Gaussian, Inc.: Wallingford CT, USA2009.

[2] S. Okamoto, K. Tanaka, Y. Izumi, H. Adachi, T. Yamaji and T. Suzuki, *Jpn. J. Appl. Phys.*, 2001, **40**, 783.

[3] T.-C. Chao, Y.-T. Lin, C.-Y. Yang, T. S. Hung, H.-C. Chou, C.-C. Wu and K.-T. Wong, *Adv. Mater.*, 2005, **17**, 992.

[4] Y. Yang, P. Cohn, S. H. Eom, K. A. Abboud, R. K. Castellano and J. Xue, *J. Mater. Chem. C*, 2013, **1**, 2867.

[5] K. Guo, J. Zhang, T. Xu, X. Gao and B. Wei, *J. Display Technol.*, 2014, **10**, 642.

[6] X. Tang, L. Yao, H. Liu, F. Shen, S. Zhang, Y. Zhang, H. Zhang, P. Lu and Y. Ma, *J. Mater. Chem. C*, 2014, **2**, 5019.